



Fast-light enhancement of an optical cavity by polarization mode coupling

David D. Smith,¹ H. Chang,² Krishna Myneni,³ and A. T. Rosenberger⁴

¹*NASA Marshall Space Flight Center, Space Systems Department, ES31, Huntsville, Alabama 35812, USA*

²*Ducommun Miltec, 678 Discovery Dr., Huntsville, Alabama 35806, USA*

³*U.S. Army AMRDEC, RDMR-WDS-WO Redstone Arsenal, Alabama 35898, USA*

⁴*Department of Physics, Oklahoma State University, 145 Physical Sciences, Stillwater, Oklahoma 74078, USA*

(Received 25 February 2014; published 5 May 2014)

We present an entirely linear all-optical method of cavity scale factor enhancement that relies on mode coupling between the orthogonal polarization modes of a single optical cavity, eliminating the necessity of using an atomic medium to produce the required anomalous dispersion, which decreases the dependence of the scale factor on temperature and increases signal-to-noise ratio by reducing absorption and nonlinear effects. The use of a single cavity results in common mode rejection of the noise and drift that would be present in a system of two coupled cavities. We show that the scale-factor-to-mode-width ratio is increased above unity for this system, and demonstrate tuning of the scale factor by (i) directly varying the polarization mode coupling via rotation of an intracavity half-wave plate, and (ii) coherent control of the cavity reflectance which is achieved simply by varying the incident polarization superposition. These tuning methods allow us to closely approach the critical anomalous dispersion condition and achieve unprecedented enhancements in scale factor and in the scale-factor-to-mode-width ratio. Based on these findings, we propose an adaptation of the traditional optical cavity gyroscope that takes advantage of polarization mode coupling to enhance the gyro scale factor, and demonstrate how the bandwidth of the scale factor enhancement for this gyroscope can be effectively broadened in comparison with fast-light gyroscopes based on atomic media.

DOI: [10.1103/PhysRevA.89.053804](https://doi.org/10.1103/PhysRevA.89.053804)

PACS number(s): 42.60.Da, 42.50.Gy, 42.81.Pa

I. INTRODUCTION

Recent experiments using atomic Rb vapor as an intracavity anomalous dispersion, or fast-light, medium have demonstrated that the scale factor of an optical cavity can be strongly enhanced as a result of mode pushing which provides a positive feedback to the cavity response [1–4]. The cavity becomes hypersensitive to variations in length at a critical value of the anomalous dispersion where a pole occurs in the cavity scale factor. The mode width does not increase to the same degree because of mode reshaping by group velocity dispersion, resulting in an overall increase in the scale-factor-to-mode-width ratio. These revelations have led to efforts to further develop these dispersion-enhanced cavities for applications such as increasing the precision of optical gyroscopes for inertial navigation [1–7], increasing the sensitivity-bandwidth product for interferometric gravity wave detectors [8–10], precision measurements of the Lense-Thirring frame-dragging effect [6], increasing the delay-bandwidth product of data buffers without distortion [11], the autostabilization of optical cavities [12,13], and enhanced strain and displacement sensing [14].

One drawback that has been pointed out for these atom-cavity systems, however, is that the increase in the scale-factor-to-mode-width ratio is accompanied by a substantial decrease in the output intensity as a result of the absorption of the atomic medium, thereby limiting the increase in the signal-to-noise ratio [15]. Additional concerns are spatial and temporal variations in scale factor as a result of the temperature dependence of the atomic absorption, as well as the presence of intensity-dependent nonlinearities which complicate the calculation of the response, tend to reduce the scale factor, and limit the signal-to-noise ratio by limiting the intensity of the input beam that can be applied.

Fortunately, the dispersion enhancement does not only occur for the case of an intracavity medium. An alternative and more fundamental way of looking at the “dispersion” enhancement is that it results from the coupling of resonant modes. In this view, the scale factor pole is simply an example of an exceptional point, commonly found in coupled systems described by non-Hermitian Hamiltonians, such as coupled oscillators having different loss rates. The dispersion enhancement can therefore be found in any physical system involving coupled oscillators near such an exceptional point [16]. Therefore, an attractive approach would be to eliminate the intracavity atomic medium entirely and instead use the resonances of a second cavity of fixed length as the intracavity dispersive element. As discussed in a previous work, to achieve the required anomalous dispersion and enhance the scale-factor-to-mode-width ratio it is necessary to undercouple the individual cavities to each other and undercouple the entire system to the incident light, respectively [17]. In practice this is easy to achieve and results in a higher signal-to-noise ratio because light that would have been absorbed and reradiated incoherently in all directions by the intracavity absorber is now coherently recycled by the additional cavity. Moreover this all-optical approach is entirely linear, does not suffer from the temperature dependency of the atomic absorption, and is not limited to operation at atomic resonance frequencies.

Producing a coupled-cavity system with a stable relative detuning between the modes of two different cavities is not a simple proposition, however, because each cavity suffers from independent amounts of noise and drift. Implementation of such a scheme therefore requires the stabilization of one cavity to the other at some controllable offset. A chief advantage of the atom-cavity systems, therefore, is the inherently stable

resonant frequencies offered by atomic systems for creating the dispersion enhancement. An additional complication is that there is no simple way to control the degree of coupling between the two cavities in order to tune the scale factor. In the case of an atom-cavity system the scale factor can be controlled by modifying the atomic absorption using temperature, magnetic field, or a second optical pumping beam applied transverse to the cavity [3]. Unfortunately, these methods cannot be used in the coupled-cavity approach because they all rely on the presence of an atomic vapor. While it is possible to use coupled fiber optic resonators with tunable couplers, these systems typically suffer from even greater noise and drift than do free space cavities [18]. In this paper, we present an alternative “coupled-cavity” approach which relies on mode coupling between orthogonally polarized modes in a single cavity. The noise and drift are common mode rejected, because both polarization modes, i.e., “cavities,” share the same optical path, resulting in a stable relative mode detuning which can be controlled by an intracavity variable retarder aligned with one of the polarization modes. Mode coupling is controlled by the simple rotation of an intracavity half-wave retarder. In this manner, the enhancement in cavity scale factor is reproducible and stable.

An additional benefit of using polarization mode coupling is that it allows investigation of an alternative method for tuning the scale factor, via coherent control of the cavity reflectance. In this case a second input beam is directed into the cavity such that it coherently interferes with the first input beam [4,19]. The tunability of the scale factor then arises from the interference between the transmission of the first input and the reflection of the second from the cavity. This approach is closely related to the recently demonstrated phenomenon of coherent perfect absorption [20,21], but differs in that it does not require increasing the cavity absorptance to unity. Instead only a slight modification of the cavity absorptance is required, which can be accomplished simply by varying the relative intensity of the second beam while keeping its relative phase constant. This method has the advantage over other scale factor tuning methods in that it is completely linear, occurs irrespective of the choice of intracavity medium, and occurs on the fast time scale of the cavity buildup time. Moreover, the scale factor can be tuned without needing to disturb or modify anything inside the cavity, which could diminish the cavity performance. This scheme is difficult to implement, however, using two different cavities because the introduction of a second coherent input beam effectively means employing an interferometer. The resulting phase fluctuations in the interferometer, along with the required active stabilization of the coupled cavities, makes the use of two different cavities impractical for demonstrating this method of tuning the scale factor. The arrangement presented herein solves these problems. The two coupled cavities are replaced by a single cavity whose polarization modes couple, enabling interference to occur between the two orthogonally polarized inputs. Hence, this arrangement allows two “inputs” into the cavity whose phase difference is stable, being determined solely by the input polarization, without having to actually inject a second coherent beam, and it results in common mode rejection of cavity noise.

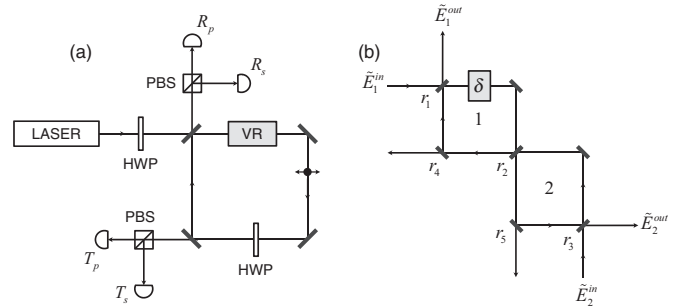


FIG. 1. (a) A tunable diode laser is scanned over the modes of a passive ring cavity to obtain s - and p -polarized reflection and transmission spectra (PBS: polarizing beam splitter). The cavity polarization modes are detuned by a variable retarder (VR) and coupled by a half-wave plate (HWP). The linear input polarization is controlled by a half-wave plate external to the cavity. (b) Equivalent coupled-cavity system, where \tilde{E}_1^{in} and \tilde{E}_2^{in} represent the two orthogonally polarized inputs.

II. EXPERIMENTAL SETUP AND MEASUREMENT OF CAVITY SCALE FACTOR

An external-cavity diode laser having a linewidth of <1 MHz at 780 nm was used to scan over the modes of an $L = 30$ cm, 1 GHz free spectral range (FSR) optical ring cavity to obtain polarized reflection and transmission spectra as shown in Fig. 1(a). An intracavity liquid crystal (LC) variable retarder whose slow (tuning) axis was aligned horizontally with the p -polarization mode was used to introduce a controllable detuning between the two orthogonal polarization modes of the cavity. An intracavity half-wave plate (HWP) whose fast axis was aligned close to the vertical direction was used to couple the polarization modes. The coupling can be turned off by positioning the wave plate in the vertical (or horizontal) direction and is maximized at 45° at which point the cavity FSR is essentially halved. An alternative method for varying the coupling would be to use a second variable retarder whose slow axis is fixed at 45° , and vary its retardance [22]. In practice we found this to be difficult because of the temperature dependence of the retardance. At this large rotation angle, the retardance difference between the coupled and uncoupled states was negligible compared with retardance changes induced by noise or temperature variations during the measurement.

III. THEORETICAL MODEL

For the purposes of modeling, the two coupled polarization modes can be treated as if they were the modes of two (stable) coupled cavities with two inputs, as shown in Fig. 1(b). This coupled-cavity model is formally identical to a Jones matrix treatment (see Appendix) where every element is represented by a diagonal Jones matrix except the half-wave plate that couples the two polarization modes. Hence, the accuracy of this model relies on the assumption that the other cavity elements do not produce any additional polarization coupling. The simple coupled-cavity model, however, is more intuitive than the Jones matrix treatment, and provides closed-form analytic expressions which enable rapid computation of the cavity response.

Much of the theory that follows was presented previously for a single input [17], but here we generalize our previous treatment to two input beams. The total single-beam complex reflection and transmission coefficients for a coupled-cavity system can be written in terms of the detuning $\Delta_L = \omega_L - \omega_q$ of the laser frequency ω_L from the q th resonance frequency of the fixed cavity ω_q by the nested relations

$$\tilde{\rho}_{13}(\Delta_L, \delta_{m,q}) = \frac{\tilde{E}_1^r}{\tilde{E}_1^{\text{in}}} = \frac{r_1 - c_1 a_1 \tilde{\rho}_{23}(\Delta_L) \exp[i\phi_1(\Delta_L, \delta_{m,q})]}{1 - r_1 a_1 \tilde{\rho}_{23}(\Delta_L) \exp[i\phi_1(\Delta_L, \delta_{m,q})]} \quad (1)$$

and

$$\tilde{\tau}_{13}(\Delta_L, \delta_{m,q}) = \frac{\tilde{E}_1^t}{\tilde{E}_1^{\text{in}}} = \frac{\tilde{t}_1 \tilde{\tau}_{23}(\Delta_L) a_1^{1/2} \exp[i\phi_1(\Delta_L, \delta_{m,q})/2]}{1 - r_1 a_1 \tilde{\rho}_{23}(\Delta_L) \exp[i\phi_1(\Delta_L, \delta_{m,q})]}, \quad (2)$$

respectively, where \tilde{E}_1^{in} , \tilde{E}_1^r , and \tilde{E}_1^t are the complex electric field amplitudes for the input, reflected, and transmitted beams for the first input; $\phi_1(\Delta_L, \delta_{m,q}) = (\Delta_L - \delta_{m,q})\tau_1 = (\omega_L - \omega_m)\tau_1$ is the round-trip phase shift accumulated in the first cavity; $\delta_{m,q} = \omega_m - \omega_q$ is the detuning of the m th mode of the first (tunable) cavity from the q th mode of the second (fixed) cavity when they are uncoupled from one another; $\tau_{1,2}$ are the round-trip times in the first and second cavities; and $a_{1,2}$ accounts for other frequency-independent round-trip losses in the first and second cavities, respectively. The reflection coefficients of the mirrors r_j are assumed to be real valued where $j = 1, 2, 3$. The mirror transmission coefficients are $\tilde{t}_j = (1 - r_j^2 - b_j^2)^{1/2} e^{i\vartheta_j} = t_j e^{i\vartheta_j}$, where b_j accounts for mirror absorption, and ϑ_j is the mirror transmitted phase shift. The quantity $c_j \equiv r_j^2 + t_j^2 = 1 - b_j^2$ represents the sum of the reflection and transmission for each component. We will assume that the coupling is conservative such that $b_2 = 0$. The transmitted phase at the two input mirrors is simply $\vartheta_{1,3} = \pi/2$, whereas the transmitted phase of the coupling element (HWP) is $\vartheta_2 = \pi$. Because of cavity misalignment, however, the latter can effectively depend on the rotation angle of the wave plate, i.e., $\vartheta_2(\theta_c)$. The coefficients of the second fixed cavity are given by similar (but not nested) relations:

$$\tilde{\rho}_{23}(\Delta_L) = \frac{r_2 - c_2 r_3 a_2 \exp[i\phi_2(\Delta_L)]}{1 - r_2 r_3 a_2 \exp[i\phi_2(\Delta_L)]} \quad (3)$$

and

$$\tilde{\tau}_{23}(\Delta_L) = \frac{\tilde{t}_2 \tilde{\tau}_{32}^{1/2} \exp[i\phi_2(\Delta_L)/2]}{1 - r_2 r_3 a_2 \exp[i\phi_2(\Delta_L)]}. \quad (4)$$

Note that the round-trip phase shift in the second cavity $\phi_2(\Delta_L) = \tau_2 \Delta_L$ does not depend on the detuning $\delta_{m,q}$, because its length does not change. And because the two cavities have the same length we can assume $\tau_2 = \tau_1$.

Now the total reflected field from the first (second) cavity is a coherent combination of the reflection of the first (second) input with the transmission of the second (first) input, i.e.,

$$\begin{aligned} \tilde{\rho}_1(\beta, \varphi) &= \tilde{E}_1^{\text{out}} / \tilde{E}_1^{\text{in}} = \tilde{\rho}_{13} + \tilde{\tau}_{31} \beta \exp(i\varphi), \\ \tilde{\rho}_2(\beta, \varphi) &= \tilde{E}_2^{\text{out}} / \tilde{E}_2^{\text{in}} = \tilde{\rho}_{31} + \tilde{\tau}_{13} \exp(-i\varphi) / \beta, \end{aligned} \quad (5)$$

where \tilde{E}_2^{in} is the electric field amplitude of the second input, and $\tilde{E}_1^{\text{out}} = \tilde{E}_1^r + \tilde{E}_2^t$ and $\tilde{E}_2^{\text{out}} = \tilde{E}_1^t + \tilde{E}_2^r$ are the field

amplitudes at the outputs. The additional factor $\beta \exp(i\varphi)$ represents the relative amplitude and phase of the second input with respect to the first, at the cavity input mirrors, i.e.,

$$\tilde{E}_2^{\text{in}} / \tilde{E}_1^{\text{in}} = \beta \exp(i\varphi). \quad (6)$$

Note that to obtain the backward-going coefficients $\tilde{\rho}_{31} = \tilde{E}_2^r / \tilde{E}_2^{\text{in}}$ and $\tilde{\tau}_{31} = \tilde{E}_2^t / \tilde{E}_2^{\text{in}}$ we simply reverse the roles of r_1 and r_3 , \tilde{t}_1 and \tilde{t}_3 , a_1 and a_2 , $\phi_1(\Delta_L, \delta_{m,q})$, and $\phi_2(\Delta_L)$, and replace \tilde{t}_2 with its complex conjugate wherever it appears in Eqs. (1)–(4).

Now, assume the first (second) cavity represents the p -polarized (s -polarized) mode, such that $\tilde{\rho}_p(\beta, \varphi) = \tilde{\rho}_1(\beta, \varphi)$ and $\tilde{\rho}_s(\beta, \varphi) = \tilde{\rho}_2(\beta, \varphi + \pi)$. When the two input directions model orthogonal polarizations, a factor of π must be added to φ for one of the polarizations because the input angle is effectively reversed with respect to the cavity upon a change in the input direction, i.e., there is a mirror image change in the reference frame. The total reflectance of the two (s - and p -polarized) inputs is then given by $R_{s,p} = |\tilde{\rho}_{s,p}|^2$, i.e.,

$$R_s = |\tilde{\rho}_{13}|^2 + \beta^2 |\tilde{\tau}_{31}|^2 + 2\beta \text{Re}\{\tilde{\rho}_{13}^* \tilde{\tau}_{31} \exp(i\varphi)\},$$

$$R_p = |\tilde{\rho}_{31}|^2 + |\tilde{\tau}_{13}|^2 / \beta^2 - 2 \text{Re}\{\tilde{\rho}_{31}^* \tilde{\tau}_{13} \exp(-i\varphi)\} / \beta. \quad (7)$$

The unlabeled mirrors in Fig. 1(b) are considered to have unity reflectance. When cavity transmission is considered, a slight modification of the above equations must be made to include the reflection coefficients r_4 and r_5 at the cavity output mirror. Calculation of the total cavity transmission through this mirror for the two polarizations is then similar to the analytical treatment given above for the cavity reflection.

Typically, the specific frequencies of the coupled polarization modes in reflection are obtained analytically by setting the derivative of Eq. (7) with respect to Δ_L equal to zero. For a single input ($\beta = 0$) these solutions are readily found, but for two inputs the interference term complicates the calculation and numerical peak finding methods are required. The detuning between the m th mode of the first cavity from the q th mode of the second cavity when the cavities (orthogonal polarizations) are coupled to one another can be defined as $\Delta_{m,q} = \Omega_m - \Omega_q$. We will only consider the interaction between two nearby modes, so we can drop mode numbers for simplicity, and from here on will refer to the coupled and uncoupled mode detunings as simply Δ and δ , respectively. The enhancement in the cavity scale factor can then be defined as $S = d\Delta/d\delta$. As discussed previously, a pole occurs in the scale factor at a critical anomalous dispersion (CAD) where the cavity becomes hypersensitive to length changes.

For a single-beam incident on a coupled cavity at least one of the individual cavities must be undercoupled to the other to achieve the required intracavity anomalous dispersion, i.e., $(r_1 < r_2/a_1) \vee (r_3 < r_2/a_2)$. Furthermore, enhancement of the scale-factor-to-mode-width ratio S/W requires that the entire coupled-cavity system be undercoupled to the incident light, i.e., $r_1 > a_1 \rho_{23}$ [17]. When a second beam is incident on the system these specific conditions are modified by the interference with the second beam, but the general condition still holds that the spectra of the individual cavities and that of the entire system (as perturbed by the second beam) should impart a phase shift that decreases with frequency, i.e., be anomalously dispersive.

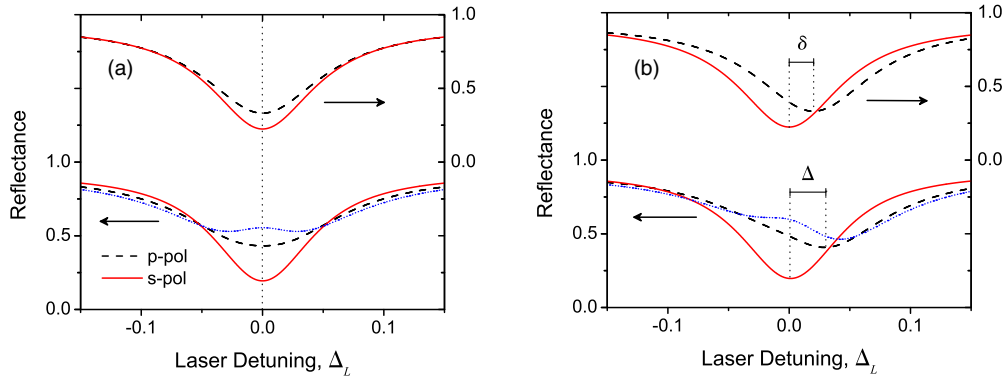


FIG. 2. (Color online) s -polarized (solid curve) and p -polarized (dashed curve) reflection spectra produced by the coupled-cavity model at (a) $\delta = 0$ and (b) $\delta = 0.02$ for coupled (bottom) and uncoupled (top) polarization modes. In this and subsequent figures, all frequencies are in units of the free spectral range. The phase shift of the coupling mirror is set to $\vartheta_2 = \pi$, which produces symmetric results about $\Delta_L = 0$ when δ is reversed in sign. The reflection coefficient of the coupling mirror is $r_2 = 0.9989$ as in Fig. 5. All other parameters are the same as described below in Sec. IV, i.e., $a_1 = 0.825$, $r_1 = 0.897$, $a_2 = 0.813$, $r_3 = 0.888$, $r_4 = 0.932$, $r_5 = 0.995$, $b_1 = 0.255$, $b_3 = 0.260$, $b_4 = 0.120$, $\beta = 1.376$, and $\varphi = 0$. In (a) mode broadening of the p -polarized mode occurs, while in (b) the scale factor is enhanced as a result of mode pushing of the p -polarized mode, i.e., $\Delta > \delta$. For the dotted curve the relative amplitude of the second input is increased to $\beta = 3.0$, which causes the p -polarized mode to split in (a) and to be pushed to a greater extent in (b). The s -polarized mode is not significantly changed and so is not shown for this case. A pole in the scale factor occurs at the CAD condition when the spectrum just splits at $\delta = 0$.

In Fig. 2 polarized reflection spectra generated by Eq. (7) are shown for coupled and uncoupled polarization modes at two different values of δ . These spectra demonstrate how the scale factor can be enhanced by mode pushing and how this pole can be approached or exceeded by variation of the coupling parameter r_2 or the relative input amplitude β . It is apparent by inspection of Eq. (7) that three terms contribute to the scale factor. The first two terms have been discussed previously [17]. The third term is the only contribution that contains the relative phase φ , and arises due to the interference between the transmission of one input beam and the reflection of the other input beam. This modification of the cavity reflection spectrum by a second input beam that is coherent with the first, is the same physical mechanism behind the recently discussed phenomenon of coherent perfect absorption [21,22], differing only in the degree of output cancellation. In the case of coherent perfect absorption, the reflection is completely cancelled. On the other hand, only a small change in reflection is needed to obtain a substantial modification of the cavity

scale factor, particularly near the CAD condition where a pole in the scale factor occurs. Importantly, as β is varied, the symmetry of the spectrum about $\Delta_L = 0$ is preserved only when $\varphi = 0$ or π . For linearly polarized incident light, this condition is automatically satisfied. When $\varphi = 0$, as β is increased, the reflectance of the cavity at $\Delta_L = 0$ increases, which in turn increases the scale factor as shown in Fig. 2. When β is sufficiently large that the scale factor pole is exceeded, the spectrum splits. For $\varphi = \pi$, the opposite occurs as β is increased (not shown). In this case, the reflectance of the cavity decreases, thereby reducing the scale factor and moving the cavity away from the CAD condition.

IV. RESULTS AND DISCUSSION

Spectra were recorded with and without mode coupling, at a variety of detunings as one polarization mode was tuned across the other. A larger number of spectra were taken near the detuning where the two polarization modes were

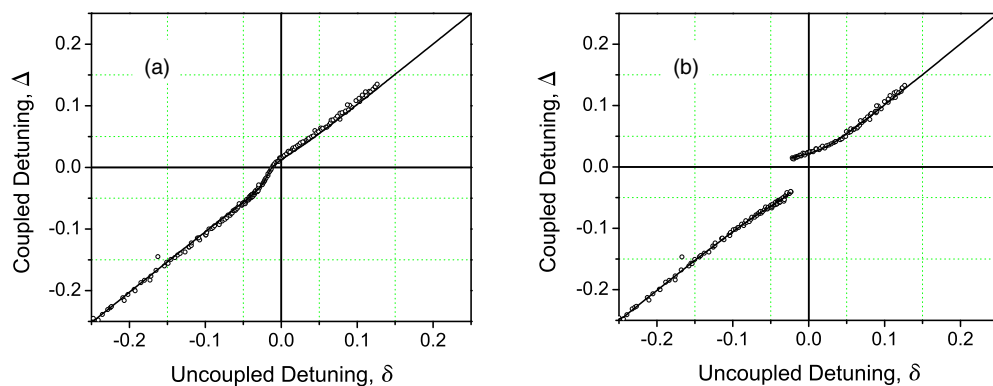


FIG. 3. (Color online) Scale factor in (a) reflection and (b) transmission. Circles represent experimental data, while solid curves represent the theoretical model. The coupling was a fitting parameter, which resulted in $\vartheta_2 = 2.4$ for both cases as well as $r_2 = 0.9985$ in (a) and $r_2 = 0.9974$ in (b).

coresonant by applying a nonlinear voltage step on the LC retarder. An automated peak finding program was written to obtain the frequencies of the mode peaks as well as their FWHM mode widths from each of the experimental spectra with the coupling turned on and off resulting in the scale factor plots shown in Fig. 3. Each data point in the figure represents a different liquid crystal voltage. The following procedure was used to obtain a comparison of the theory with the experimental data: First, the reflection coefficients at the transmission port were obtained by direct measurement to be $r_4 = 0.932$ and $r_5 = 0.995$. Measurements of the mirror absorption yielded $b_1 = 0.255$, $b_3 = 0.260$, $b_4 = 0.120$, and $b_5 = 0.060$. Next, at an arbitrary value of δ the uncoupled reflection and transmission spectra for the p -polarized modes were fit to the theory using a_1 and r_1 as fitting parameters. Similarly, the spectra for the s -polarized modes were fit to the theory using a_2 and r_3 as fitting parameters. The best-fit values from the transmission and reflection spectra were slightly different and therefore average values were determined. This procedure yielded $a_1 = 0.825$, $r_1 = 0.897$, $a_2 = 0.813$, and $r_3 = 0.888$. For comparison, direct measurements of the mirror coefficients yielded $r_1 = 0.906$ and $r_3 = 0.903$. Therefore, the two “cavities” were undercoupled to each other and the system was undercoupled to the incident light as required to obtain an enhancement in the scale-factor-to-mode-width ratio. The cavity finesse was measured from the uncoupled s -polarized reflection spectra to be $F = 9$. The finesse of the uncoupled p -polarized modes was only slightly smaller. The relative amplitude between the s - and p -polarized inputs was found from the incident linear polarization angle $\theta_i = 36^\circ$ (with respect to the vertical) to be $\beta = \cos \theta_i / \sin \theta_i = 1.376$ (more s than p polarization was incident on the cavity). For incident light that is linearly polarized, the relative phase of the inputs φ is either zero or π , depending on the orientation of the input wave plate θ_i with respect to that of the coupling wave plate θ_c . The relative phase is zero when the sines of these angles have the same sign, and π otherwise. In our case $\varphi = 0$. As noted previously, for the s -polarized (or backward-going) input, we must add a factor of $\pi \tau \varphi$ in the second equation in Eqs. (5), because the orientation of the coupling wave-plate angle is effectively reversed with respect to the second input.

Next, theoretical scale factor curves were produced using the values determined above and were fit to the data for both the reflection and the transmission, with the coupling reflection coefficient r_2 as a parameter as shown in Fig. 3. This procedure yielded best-fit values of $r_2 = 0.9985$ and $r_2 = 0.9974$, respectively. In the experiment, however, the coupling wave plate was set to $\theta_c = 1^\circ$, corresponding to $r_2 = \cos(2\theta_c) = 0.9994$. The fact that the best-fit values were larger than expected was likely due to a small residual coupling that could not be completely zeroed out even when the wave plate was rotated to the vertical position. This observation and the discrepancies in these values suggest that other sources of polarization coupling that are not accounted for by the simple coupled-cavity model exist within the cavity.

Note that near the coresonance condition, the maximum scale factor enhancement of the reflection is $S_{\max} = 3.0$, whereas mode splitting is observed in the transmission, because the CAD condition is different for reflection and transmission. The p -polarized mode (the mode being tuned)

experiences the majority of the mode pushing and reshaping. The s -polarized mode is also modified, but to a substantially lesser degree because of the relatively large value of β and because it is closer to critical coupling (see Fig. 2). Hence, the overall result is that the modes are pushed away as they approach one another, leading to an increase in S . Rotating either the coupling wave plate or the input wave plate in the opposite direction such that $\varphi = \pi$ reverses the effect and the scale factor decreases. The asymmetry of the mode splitting and offset of the enhanced scale factor region from $\delta = 0$ in Fig. 3 is a result of a slight mode asymmetry that occurs as a result of cavity misalignment, which effectively causes the detuning between the modes to change as the coupling is varied by rotation of the wave plate. This effect can be taken into account in the theoretical model via the coupler transmitted phase ϑ_2 . The value of ϑ_2 was adjusted until the offset due to the asymmetry matched that of the data, which occurred at a value of $\vartheta_2 = 2.4$. Reversing the sign of ϑ_2 also reverses the offset about $\delta = 0$.

The FWHM mode widths of the s - and p -polarized modes as the detuning between them is varied are shown in Fig. 4. Mode broadening is observed for the p -polarized mode, whereas a slight mode narrowing occurs for the s -polarized mode. The s -polarized mode experiences the opposite effect from that of the p -polarized mode because of the factor of π that must be added to φ in the second equation in Eq. (5) from the change in reference frame. Note that the increase in the mode width for the p -polarized mode as a result of the dispersion is less than $W_p = 1.5$, where W is the mode width normalized to its off-resonance value. Hence, the scale factor is increased by a factor that is larger than the mode width, resulting in an overall increase of at least $S/W = 2$.

To demonstrate coherent control of the scale factor, the incident linear polarization angle θ_i was varied while keeping the angle of the coupling wave plate θ_c constant as shown in Fig. 5. Three input angles were chosen: $\theta_i = 45^\circ$, $\theta_i = 30^\circ$, and $\theta_i = 24^\circ$, corresponding to $\beta = 1.00$ (equal input intensities), $\beta = 1.73$, and $\beta = 2.25$, respectively. Note that as the value of β increases, the scale factor for the reflected beam also

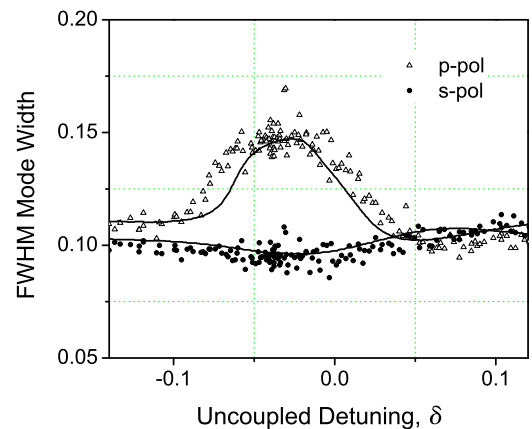


FIG. 4. (Color online) FWHM mode widths for p -polarized (top) and s -polarized (bottom) modes in reflection. Solid curves represent the theoretical model. Dots are experimental data. The mode width increase (decrease) near the coresonance detuning ($\delta = 0$) is due to mode pushing (pulling).

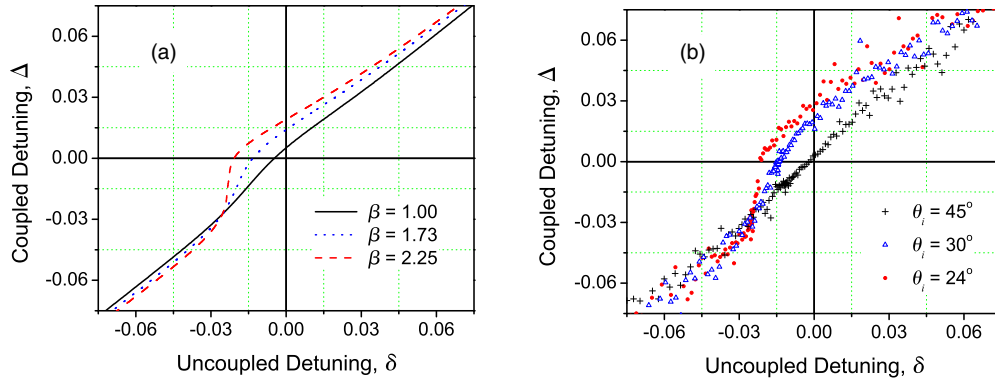


FIG. 5. (Color online) Tuning by coherent control of the cavity scale factor: (a) theoretical model and (b) experimental data. The scale factor for reflection increases as the relative amplitude of the second input beam β increases via rotation of the input polarization. The coupling parameter was $r_2 = 0.9989$. All other parameters are the same as described previously.

increases due to the interference with the second input beam. The interference effectively attenuates the mode, increasing the effect of the anomalous dispersion introduced by the coupling to the s -polarized cavity mode (see Fig. 2). At $\theta_i = 45^\circ$ the scale factor is not enhanced, i.e., $S = 1.0$, whereas at $\theta_i = 24^\circ$ the enhancement was measured to be $\bar{S} = 8.3$ by making a linear fit to only the points residing in the linear regime close to the resonance. This procedure results in an average (rather than maximum) scale factor in the regime close to resonance. Hence, without modifying or disturbing any intracavity elements the scale factor can be tuned over a large range merely by changing the input polarization superposition.

In Fig. 6 an attempt was made to obtain the largest possible scale factor within the experimental constraints to demonstrate the pole in the scale factor that occurs at the CAD condition. The cavity was realigned to minimize misalignment, the transmission path was eliminated by replacing the output coupler with a high reflector such that $r_4 = r_5 = 1$, and the coarse wave-plate mounts were replaced with precision rotation mounts to hone in on the scale factor pole. Note that the offset of the data from $\delta = 0$ has the opposite sign and is now smaller than it was in Fig. 3 as a result of the improved alignment. The new value of the finesse measured for the uncoupled s -polarized modes was $F = 10$. The input polarization was set to $\theta_i = 24^\circ$ ($\beta = 2.25$), the

coupling wave plate was set at $\theta_c = 3^\circ$ (corresponding to $r_2 = 0.9945$), and the wave plates were finely tuned over a few arc minutes until the spectrum, observed on an oscilloscope, came very close to splitting. Data were then recorded over a small region around $\delta = 0$. The resulting average scale factor enhancement near coresonance was measured to be $\bar{S} = 28.3 \pm 1.0$. The mode width of the p -polarized modes increased by only $\bar{W}_p = 1.85 \pm 0.003$, whereas the mode width of the s -polarized modes was almost unchanged at $\bar{W}_s = 0.94 \pm 0.002$. Hence, the scale-factor-to-mode-width ratio was enhanced by $\bar{S}/\bar{W}_p = 15.2 \pm 1.0$.

V. POLARIZATION-COUPLED PASSIVE FAST-LIGHT OPTICAL GYROSCOPE

In this section we propose a passive optical gyroscope that takes advantage of polarization mode coupling to produce anomalous dispersion, resulting in an enhancement of the gyro scale factor. A general schematic of the setup is shown in Fig. 7. In this arrangement, the cavity modes of both polarizations split as a result of the rotation, but the electro-optic modulator (EOM) creates an index difference between the s and p polarizations which results in different amounts of mode splitting for the two polarizations. The polarization mode that splits less, enhances the splitting of the mode that splits

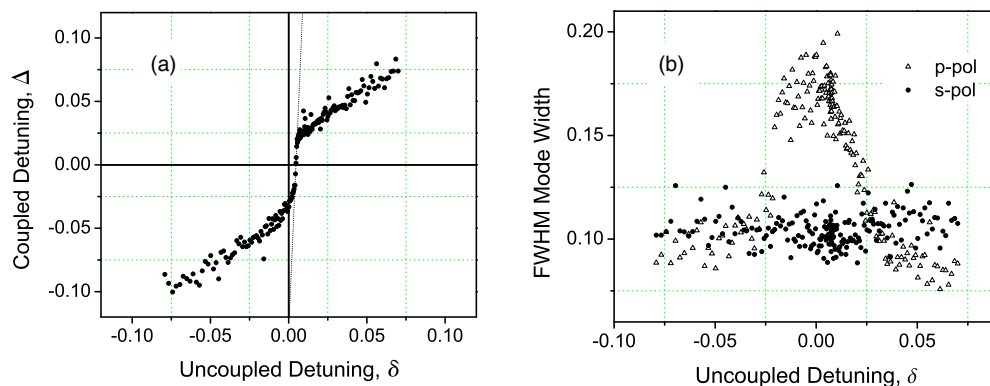


FIG. 6. (Color online) (a) A pole in the scale factor becomes evident near the critical anomalous dispersion condition. The dotted line is the result of a linear fit to points lying in the region of enhanced scale factor. (b) FWHM mode widths.

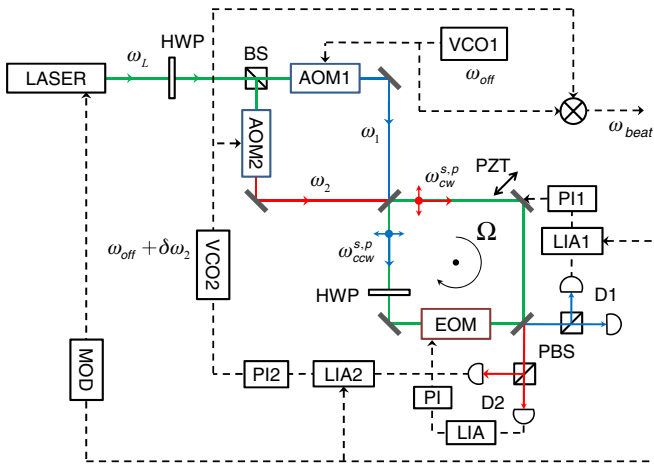


FIG. 7. (Color online) A passive fast-light optical gyroscope based on polarization mode coupling. Rotation of the gyro at frequency Ω splits the cavity modes into clockwise and counterclockwise frequencies $\omega_{cw}^{s,p}$ and $\omega_{ccw}^{s,p}$ for each polarization. A laser at frequency ω_L is shifted by some offset frequency ω_{off} by two AOMs, one of which is fixed in frequency (AOM1). The cavity mode frequency at one polarization, ω_{ccw}^s , is locked to the light generated by AOM1 at $\omega_1 = \omega_L + \omega_{off}$ by the PZT, while the light passing through AOM2 at $\omega_2 = \omega_L + \omega_{off} + \delta\omega_2$ is locked to ω_{cw}^s by adjusting VCO2. In addition, ω_{ccw}^p is locked to ω_{cw}^s by adjusting the EOM, whose tuning axis is horizontal. The signals from VCO1 and VCO2 are mixed to determine the beat frequency ω_{beat} . (HWP: half-wave plate; AOM: acousto-optic modulator; LIA: lock-in amplifier; PI: proportional integral servo controller; VCO: voltage controlled oscillator; PZT: piezoelectric transducer; EOM: electro-optic modulator; PBS: polarization beam splitter; BS: beam splitter; D: detector array.)

more, resulting in an increased beat frequency measurement. The feedback system only tracks the enhanced polarization mode (the s -polarization mode in the figure), which functions the same as for a traditional passive gyroscope, i.e., one of the counterpropagating cavity modes is locked via a piezoelectric transducer (PZT) to input light that is frequency shifted by a fixed-frequency acousto-optic modulator (AOM), while light from the other input is locked to the opposite cavity mode by adjusting the frequency of a second variable-frequency AOM. In contrast with passive fast-light gyroscopes based on atomic media, the AOM offset frequency can be set to any value and there is no need to stabilize the input laser frequency to the anomalous dispersion resonance. The polarization mode that is not enhanced (the p -polarization mode in the figure) is stabilized to the enhanced (s -polarized) mode in one of the two counterpropagating directions (the clockwise direction in the figure) using the EOM (whose tuning axis is along the p -polarized direction). The p -polarized mode in the opposite direction (counterclockwise in the figure) is not locked and simply pushes on the counterclockwise s -polarized mode. In contrast with the dispersion provided by atomic resonances, in this case the dispersive feature (the p -polarized mode) is not fixed but follows the s -polarized mode, continually pushing on it as the rotation rate varies. Because both polarization modes shift similarly in frequency, the bandwidth of the scale factor enhancement is effectively broadened in

comparison with fast-light gyroscopes based on atomic media, which utilize anomalous dispersion features that are fixed in frequency.

VI. CONCLUSION

We have demonstrated an entirely linear all-optical method of cavity scale factor enhancement using mode coupling between the orthogonal polarization modes of a single optical cavity. Eliminating the atomic medium decreases the variation of the scale factor with temperature, reduces absorption and scattering of radiation from the cavity, and eliminates saturation effects, thereby increasing the signal-to-noise ratio. The approach is not limited to operation at atomic resonance frequencies. Moreover, the use of a single cavity results in common mode rejection of noise and drift, enabling demonstration of the scale factor enhancement without the need to mutually stabilize two cavities. By eliminating variations that occur in the relative phase of the two cavity input beams, this arrangement also enables demonstration of coherent control of the cavity scale factor. The advantage of this method is that it enables rapid tuning (fundamentally limited only by the cavity buildup time) of the scale factor to the optimal fast-light condition without having to disturb anything inside the cavity. We have shown that the scale factor can be readily tuned either by rotating the coupling half-wave plate, or by rotation of the input polarization. These tuning mechanisms have allowed us to closely approach the CAD condition, achieving a scale factor enhancement of $\bar{S} = 28.3 \pm 1.0$ and a scale-factor-to-mode-width ratio of $\bar{S}/\bar{W}_p = 15.2$. Automation of the peak finding procedure and the use of nonlinear data steps has allowed substantially more data to be collected in the region of scale factor enhancement, significantly reducing the uncertainty in comparison with our previous measurements [3].

We have proposed a polarization-coupled passive gyroscope design based on these effects with the potential for scale factor enhancements over a larger bandwidth than can be achieved in passive fast-light gyroscopes based on atomic media, and with larger enhancements in the scale-factor-to-mode-width ratio. For atomic passive fast-light optical gyroscopes, when the mode width (which is broadened by the anomalous dispersion) is much narrower than the atomic linewidth, the dispersion is approximately linear in a region near the dispersive resonance, and the reshaping of the mode due to group velocity dispersion can be neglected. In this linear dispersion regime the scale-factor-to-mode-width ratio is not increased above unity [1,6,14]. The linear dispersion regime only applies at small scale factor enhancements, however, for the following reason. Consider that to be in the linear regime the entire cavity mode, not just the peak, must be well within the dispersive resonance width at all detunings of interest, even at the CAD condition. But at the CAD condition, the mode width must become infinite according to the linear analysis, placing the mode outside the linear regime. Therefore, at high enough scale factors, the cavity will always be outside the linear dispersion regime, where higher order dispersion simultaneously augments the mode pushing (by reshaping the mode) and limits the mode broadening, resulting in an enhancement in S/W . As an example, consider a dispersive linewidth $\Gamma = 500$ MHz (roughly the Doppler broadened Rb⁸⁷

D_2 linewidth) and a mode width $W = 500$ kHz (corresponding to a finesse of 2000 for a 1 GHz, 30-cm-long cavity). To be in the linear regime the cavity mode width must be $W + 2\Omega_{\max} \ll \Gamma/S$, where Ω_{\max} is the magnitude of the largest rotation induced frequency shift of interest. Therefore, the scale factor enhancement must be $S \ll 10^3$ to be in the linear regime. Hence, at larger dispersive linewidths and higher values of the cavity finesse, it becomes progressively more difficult (one must go to higher scale factors) to enhance the scale-factor-to-mode-width ratio of a passive cavity containing an atomic medium, owing to the absence of higher order dispersion. Narrower atomic resonances can of course be used to increase the higher order dispersion. This is not a concern at all, however, for the proposed polarization-coupled fast-light gyro, because the two mode widths are comparable. Under these conditions it is not possible to be in the linear dispersion regime even at small scale factors. The similarity in mode widths reduces the coupling required to reach the CAD condition (only a few degrees of rotation of the intracavity wave plate were required) and provides strong higher order dispersion that results in an immediate enhancement in S/W . On a final note, it may also be possible to develop an active polarization-coupled laser gyroscope by using orthogonally polarized subthreshold cavity modes that push on the lasing modes.

ACKNOWLEDGMENTS

This work was sponsored by the NASA Office of Chief Technologist Game Changing Development Program and the U.S. Army Aviation and Missile Research Development and Engineering Center (AMRDEC) Missile S&T Program. The participation of ATR was sponsored by the Summer Research and Travel Program of the Oklahoma State University College of Arts and Sciences.

APPENDIX: JONES MATRIX TREATMENT

The coupled polarization mode cavity can be treated using the Jones matrix formalism. Given an input Jones vector \mathbf{J}_{in} , which specifies the polarization state of the light incident on the input mirror in Fig. 1(a), the Jones vectors for the field in transmission and reflection, \mathbf{J}_t and \mathbf{J}_r , respectively, can be calculated. We define a composite Jones matrix

$$\mathbf{M}_1 = \mathbf{A}_q \mathbf{T}_{L2} \mathbf{A}_h \mathbf{R}_m^2 \mathbf{T}_{L1}, \quad (\text{A1})$$

where \mathbf{T}_{L1} and \mathbf{T}_{L2} are the Jones matrices through the first (variable) and second (HWP) retarders, respectively, \mathbf{R}_m is the Jones matrix for reflection from any mirror other than those for the transmitted and reflected beams, and $\mathbf{A}_h = \mathbf{A}_{\text{RT}}^{1/2}$ and $\mathbf{A}_q = \mathbf{A}_{\text{RT}}^{1/4}$ are diagonal Jones matrices that account for polarization-dependent losses distributed over a half and

quarter round-trip, respectively. \mathbf{A}_{RT} is the total round-trip polarization-dependent loss in the cavity. We also denote the Jones matrices in transmission at the input and output couplers of the ring cavity to be \mathbf{T}_{B1} and \mathbf{T}_{B2} , respectively, and the Jones matrices in reflection at the input and output couplers to be \mathbf{R}_{B1} and \mathbf{R}_{B2} , respectively.

For the transmission port, the effective round-trip Jones matrix inside the ring cavity is given by

$$\mathbf{M}_{\text{RT1}} = \exp(i\phi_R) \mathbf{M}_1 \mathbf{R}_{B1} \mathbf{A}_q \mathbf{R}_{B2}, \quad (\text{A2})$$

where ϕ_R is the overall round-trip phase shift through the empty cavity. The Jones vector in transmission from the cavity is then given by the relations

$$\begin{aligned} \mathbf{J}_t &= \mathbf{T}_{B2} \sum_{i=1}^{\infty} \mathbf{J}_5^{(i)}, \\ \mathbf{J}_5^{(1)} &= \exp(i3\phi_R/4) \mathbf{M}_1 \mathbf{T}_{B1} \mathbf{J}_{\text{in}}, \\ \mathbf{J}_5^{(i)} &= \mathbf{M}_{\text{RT1}} \mathbf{J}_5^{(i-1)}, \quad i > 1. \end{aligned} \quad (\text{A3})$$

Similarly, for the reflection port the effective round-trip Jones matrix inside the ring cavity is

$$\mathbf{M}_{\text{RT2}} = \exp(i\phi_R) \mathbf{A}_q \mathbf{R}_{B2} \mathbf{M}_1 \mathbf{R}_{B1}. \quad (\text{A4})$$

The Jones vector in reflection from the cavity is then given by the relations

$$\begin{aligned} \mathbf{J}_r &= \mathbf{T}_{B1} \sum_{i=1}^{\infty} \mathbf{J}_6^{(i)} - \mathbf{R}_{B1} \mathbf{J}_{\text{in}}, \\ \mathbf{J}_6^{(1)} &= \exp(i\phi_R/4) \mathbf{A}_q \mathbf{R}_{B2} \mathbf{J}_5^{(1)}, \\ \mathbf{J}_6^{(i)} &= \mathbf{M}_{\text{RT2}} \mathbf{J}_6^{(i-1)}, \quad i > 1. \end{aligned} \quad (\text{A5})$$

The advantage of the Jones matrix treatment is that it is general enough to include polarization coupling and polarization-dependent losses by each of the various individual elements that constitute the cavity. The coupled-cavity model, on the other hand, assumes that polarization coupling occurs only at the HWP, i.e., that every matrix except \mathbf{T}_{L2} is diagonal. As a result of the commutation of diagonal matrices, the polarization-dependent losses occurring at each element can be distributed up to, but not across, the HWP. It is then valid to represent the polarization-dependent losses in the two cavity sections by the diagonal matrices \mathbf{A}_h and \mathbf{A}_q as shown in the treatment above. We obtained complete agreement between the two models under these circumstances. Finally, it is worthwhile to note that while the series expressions for \mathbf{J}_t and \mathbf{J}_r have an infinite number of terms, in practice we find that computation of the first 40 terms is adequate for comparison of the models at the precision of our experiments.

- [1] D. D. Smith, K. Myneni, J. A. Odotola, and J. C. Diels, *Phys. Rev. A* **80**, 011809(R) (2009).
 [2] D. D. Smith, K. Myneni, J. A. Odotola, and J. C. Diels, in *Advances in Optical Sciences Congress*, OSA Technical Digest

- (CD), paper SMB2 (Optical Society of America, Washington, DC, 2009).
 [3] K. Myneni, D. D. Smith, J. A. Odotola, and C. A. Schambeau, *Phys. Rev. A* **85**, 063813 (2012).

- [4] D. D. Smith, K. Myneni, H. Chang, A. Toftul, C. A. Schambeau, J. A. Odutola, and J. C. Diels, in *Advances in Slow and Fast Light V*, Proceedings of the SPIE, San Francisco, California, edited by S. M. Shahriar and F. A. Narducci, Vol. 8273 (SPIE, San Francisco, 2012), p. 82730T.
- [5] U. Leonhardt and P. Piwnitski, *Phys. Rev. A* **62**, 055801 (2000).
- [6] M. S. Shahriar, G. S. Pati, R. Tripathi, V. Gopal, M. Messall, and K. Salit, *Phys. Rev. A* **75**, 053807 (2007).
- [7] H. N. Yum, M. Salit, J. Yablon, K. Salit, Y. Wang, and M. S. Shahriar, *Opt. Express* **18**, 17658 (2010).
- [8] M. Salit, G. S. Pati, K. Salit, and M. S. Shahriar, *J. Mod. Opt.* **54**, 2425 (2007).
- [9] M. S. Shahriar and M. Salit, *J. Mod. Opt.* **55**, 3133 (2008).
- [10] M. Salit and M. S. Shahriar, *J. Opt.* **12**, 104014 (2010).
- [11] H. N. Yum, M. E. Kim, Y. J. Jang, and M. S. Shahriar, *Opt. Express* **19**, 6705 (2011).
- [12] M. D. Lukin, M. Fleischhauer, M. O. Scully, and V. L. Velichansky, *Opt. Lett.* **23**, 295 (1998).
- [13] D. D. Smith, H. Chang, L. Arissian, and J. C. Diels, *Phys. Rev. A* **78**, 053824 (2008).
- [14] G. S. Pati, M. Salit, K. Salit, and M. S. Shahriar, *Opt. Commun.* **281**, 4931 (2008).
- [15] M. Salit, K. Salit, and P. Bauhahn, *Opt. Express* **19**, 25312 (2011).
- [16] In a publication by M. Terrel, M. J. F. Dignonnet, and S. Fan, *Laser Photon. Rev.* **3**, 452 (2009), the authors find that an enhancement in sensitivity is not possible in coupled cavities. However, in their analysis all the cavities have the same loss rate, precluding the existence of an exceptional point.
- [17] D. D. Smith, K. Myneni, and H. Chang, in *Advances in Slow and Fast Light VI*, Proceedings of the SPIE, San Francisco, California, edited by S. M. Shahriar and F. A. Narducci, Vol. 8636 (SPIE, San Francisco, 2013), p. 86360F.
- [18] D. D. Smith, N. N. Lepeshkin, A. Schweinsberg, G. Gehring, R. W. Boyd, Q-Han Park, H. Chang, and D. J. Jackson, *Opt. Commun.* **264**, 163 (2006).
- [19] D. D. Smith, K. Myneni, H. Chang, and J. A. Odutola, 42nd Annual Meeting of the APS Division of Atomic, Molecular, and Optical Physics, Atlanta, Georgia, Abstract BAPS.2011.DAMOP.Q1.118 (American Physical Society, Atlanta, 2011), Bull. Am. Phys. Soc. Vol. 56.
- [20] Y. D. Chong, L. Ge, H. Cao, and A. D. Stone, *Phys. Rev. Lett.* **105**, 053901 (2010).
- [21] W. Wan, Y. Chong, L. Ge, H. Noh, A. D. Stone, and H. Cao, *Science* **331**, 889 (2011).
- [22] R. J. C. Spreeuw, N. J. van Druten, M. W. Beijersbergen, E. R. Eliel, and J. P. Woerdman, *Phys. Rev. Lett.* **65**, 2642 (1990).